Simulations of Ar Gas-Puff Z-Pinch Radiation Sources with Double Shells and Central Jets on the Z Generator

V. Tangri[1], A. J. Harvey-Thompson[2], J. L. Giuliani[3], J. W. Thornhill[3], A. L. Velikovich[3], J. P. Apruzese[4], N. D. Ouart[3], A. Dasgupta[3], B. Jones[2] and C.A. Jennings[2]

[1]*Berkeley Research Associates, Beltsville MD, U.S.A.*
[2]*Sandia National Laboratories, Albuquerque, NM U.S.A.*
[3]*Plasma Physics Division, Naval Research Laboratory, Washington, DC, U.S.A.*
[4]*Consultant to the NRL through Engility Corp., Chantilly VA, U.S.A.*

Radiation-magnetohydrodynamic simulations using the non-LTE Mach2-TCRE code in (r, z) geometry are performed for two pairs of recent Ar gas-puff Z-pinch experiments on the refurbished Z generator with an 8 cm diameter nozzle. One pair of shots had an outer-to-inner shell mass ratio of 1:1.6 and a second pair had a ratio of 1:1. In each pair one of the shots had a central jet. The experimental trends in the Ar K-shell yield and power are reproduced in the calculations. However, the K-shell yield and power are significantly lower than the other three shots for the case of a double-shell puff of 1:1 mass ratio and no central jet configuration. Further simulations of a hypothetical experiment with the same relative density profile of this configuration, but higher total mass, show that the coupled energy from the generator and the K-shell yield can be increased to levels achieved in the other three configurations, but not the K-shell power. Based on various measures of effective plasma radius, the compression in the 1:1 mass ratio and no central jet case is found to be less because the plasma inside the magnetic piston is hotter and of lower density. Because of the reduced density, and the reduced radiation cooling (which is proportional to the square of the density), the core plasma is hotter. Consequently, for the 1:1 outer-to-inner shell mass ratio, the load mass controls the yield and the center jet controls the power.

I. INTRODUCTION

The physics of radiation emission, stagnation and thermalization in high energy density (HED) plasmas is of continuing interest. High current, gas-puff Z-pinches are an excellent way to produce radiating HED plasmas in the laboratory. In a gas-puff Z-pinch plasma, the voltage across the puff initiates a breakdown in the gas and the resultant current density ($\boldsymbol{J}$) combines with the magnetic field ($\boldsymbol{B}$) to form the radially inward force ($\propto \boldsymbol{J}\times\boldsymbol{B}$) that compresses the plasma onto the axis. The stagnated hot, dense, pinched plasma provides an intense radiation source. Z-pinch plasmas are optically thick and radiation transport is of comparable importance to magneto-hydrodynamics (MHD), atomic physics, and other transport processes. A recent review of gas-puff pinches can be found in Ref. [1].

Argon gas-puff implosions on the pulsed power Z generator at Sandia National Laboratories (SNL) are a demonstrated efficient source of K-shell X-rays (>3 keV). Sze *et al*.,[2] performed the first gas-puff experiments on Z at ~20 MA peak short circuit current. To inject the Ar gas into the load region, a nozzle designed by Maxwell Physics International (MPI) that produced two coaxial annular gas shells was used.[3] At the nozzle exit plane the radii of the inner shell extended from 1 to 2 cm and the outer shell extended from 3 to 4 cm. In reference to the radii of the nozzle openings, this design is referred to as $r_N = 1\text{–}2/3\text{–}4$ cm. The plenum pressures were chosen to produce the same mass in each shell, i.e., the outer-to-inner shell mass ratio was 1:1. The total linear mass loading (m_ℓ) was varied from 0.8 to 1.2 mg/cm in a five shot scan. The best shot (Z663) had the maximum Ar K-shell yield (Y_K) of 274 kJ and peak K-shell power (P_K) of 14.4 TW. Coverdale *et al*.,[4] later increased Y_K to ~300 kJ and increased P_K in shot Z1590 with the same nozzle. Comparison of the shot details in Table I shows that the pinch length (ℓ) for Z1590 was 33% longer than for Z663, but m_ℓ, the peak measured current near the load (I_{pk}), the implosion times (Δt_{imp}), and the K-shell pulse width (Δt_K) were quite similar. Even though the yields are similar, Apruzese *et. al*., [5] determined from spectroscopic analysis of the K-shell emission lines that the plasma conditions at stagnation are very different between Z1590 and Z663. This difference suggests that the plasma conditions at stagnation can be affected by small changes in the initial conditions. In 2007 the Z facility was refurbished and the peak short circuit current was increased to ~26 MA. The initial gas-puff shots on the refurbished Z generator (here termed ZR) were performed at low Marx charging voltage in order to safely test the operation of a different 8 cm diameter nozzle (though also with $r_N = 1\text{–}2/3\text{–}4$ cm) developed by Alameda Applied Sciences Corporation[6] (ASSC). The outer-to-inner shell mass ratio was chosen to be 1:1.6 based on predictions form MACH2-TCRE radiation-MHD simulations indicating that a higher mass in the inner shell would provide a greater

yield.[7] Even at low charging voltage, shot Z2381 produced Y_K ~250 kJ and P_K ~17 TW.[8] Based on this success, three Ar gas-puff shots were subsequently performed by Jones *et al*.,[9] with increased charging voltage and increased mass, but with the same 1:1.6 outer-to-inner shell mass ratio. The Ar K-shell yield was remarkably repeatable: an average of 330 kJ with only a ±9% shot-to-shot variation and a maximum value of 363 kJ for shot Z2560. Details for the shots Z2381 and Z2560 are also listed in Table I.

The motivation for a larger linear mass in the inner shell compared to that in the outer shell is to limit the disruption caused by the Magnetic Rayleigh-Taylor (MRT) instability. In an imploding Z-pinch plasma the direction of the effective gravity points form the swept-up gas layer outward toward the driving piston, which is the magnetic field in the vacuum. The sausage mode (m = 0) is the fastest growing one in this unstable configuration and the number of e-foldings for this instability increases with the initial radius as $2\sqrt{\pi r_o / \Delta r}$, where Δr is the thickness of the layer. Theoretical studies indicated that tailoring the initial gas profile to rise toward the axis could mitigate the MRT instability. Velikovich *et al*.,[10] proposed that if the initial density profile varied as $1/r^3$, then the swept-up gas layer will initially accelerate as the current (I) increases, but then decelerate near the peak of I where it is nearly constant. This deceleration reverses the growth of the MRT instability. If near the axis there is a vacuum region, then once past the peak of the density, the shell would once more accelerate toward the axis and gain kinetic energy. If the vacuum gap is not too large, the MRT growth would be limited and not disrupt the shell. A different profile to mitigate the MRT instability was developed in the work by Hammer *et al.*[11]. If one imposes the constraint of a constant inward velocity, then the 0D snowplow model [1] in conjunction with a circuit model for the generator can be used to find the exact density profile that satisfies the velocity constraint. The resulting density profile has a sharp peak on axis.

Both of the above tailored gas density profiles, the inverse power law with a central gap and the other with a strong central peak, are nearly ideal, but have only been approximated in existing Ar gas-puff experiments. The power law density profile with a vacuum gap at the axis is analogous to a double-shell gas puff with the inner shell having a significantly larger mass. The Ar gas-puff shots Z2381 and Z2560 in Table I adhere to this configuration. The centrally peaked density profile is analogous to a double-shell gas puff with a massive central jet. The L-3 Titan Pulse Sciences Division (TPSD) produced such a triple nozzle for Ar radiation source experiments early this century.[12] At the exit plane the opening for the central jet had a 0.5 cm radius, the inner shell spanned 2–3 cm, and the outer shell spanned 5–6 cm ($r_N = 0.5/2–3/5–6$ cm).[13] Each opening could be separately controlled and had its own plenum. We note four experiments in Table I with the TPSD triple nozzle fielded on two different generators that highlight the impact of the center jet on Y_K. Sze *et al*.,[14] compared several gas-puff configurations on the Double-EAGLE (DE) generator in long pulse mode. The double-shell ("outer-on-inner") shot DE5417 produced less than half the K-shell yield and power of the double shell plus center jet ("outer-on-inner-on-jet") shot DE5556. The parameters m_ℓ, I_{pk}, and Δt_{imp} were similar for both shots and both shots had an outer-to-inner shell mass ratio of 1:1.[13] The mass of the center jet was 20% of the total. Since the number of MRT e-foldings scales as $\sqrt{r_o}$, the large diameter puff would normally be very susceptible to the MRT disruption, so the successful outer-on-inner-on-jet configuration was described as a "pusher-stabilizer-radiator" platform. The concept of the central jet as the primary Ar radiator was also proposed by Chuvatin *et al.*[15]. In the 1D simulations of Chuvatin *et al*. the central fill is initially shock heated by the outer shell (pusher) and then further heated by quasi-adiabatic compression. The TPSD nozzle was also fielded on the Decade-Quad (DQ) generator in long pulse mode as listed in the last two rows of Table I. Shot DQ549 by Young *et al.*[16] was a double-shell load, and based on the reported pressure ratio of the two plenums and the planar laser-induced fluorescence

data in Ref.[13], the mass ratio of the two shells was close to 1:1. As on DE, the double-shell shot DQ549 produced less than half the K-shell yield and power of the double shell plus center jet shot DQ563. These two pairs of shots on two generators of different currents demonstrate that the addition of central jet with 20% total mass to a double shell of large diameter (12 cm) and outer-to-inner shell mass ratio 1:1 significantly enhances the Ar K-shell yield and power for long implosion times (> 200 ns). The gas-puff shots on the Z and ZR generators mentioned above were all double shells, so the question arises as to whether the Ar K-shell yield and/or power would be improved with the addition of a central jet on the shorter pulse ZR generator (~120 ns current rise time).

An investigation on the impact of a central jet in Ar gas-puff pinches on the refurbished Z generator was recently completed by Harvey-Thompson *et al*.[17]. These experiments exercised the capability to produce a central jet on the AASC 8 cm nozzle (r_N = 0.5/1–2/3–4 cm) used in Refs. [8] and [9]. Table II lists four shots and the experimental data of relevance to the role of a central jet for Ar K-shell yield on ZR: mass configuration of the gas puff; m_ℓ; total radiation yield (Y_{tot}); Y_K; peak total power (P_{tot}); P_K; and Δt_K. Shot Z2560 from Table I is included in Table II as part of the set for study. The three remaining shots are from Harvey-Thompson, *et al*.[17] In all four shots the linear mass of the outer shell was 0.385 mg/cm. Shot Z2605 has the same outer-to-inner shell mass ratio as Z2560 (1/1.6), but has an additional 0.2 mg/cm in a central jet. The fraction of total mass in the jet of Z2605 is ~17%. Shots Z2628 and Z2604 are analogous to the first pair in that the former has no center jet while the latter has one of 0.2 mg/cm. For these last two entries the inner and outer shells have equal mass, just as the first Ar gas-puff shots in Ref. [2] on pre-refurbished Z. The fraction of total mass in the jet of Z2604 is 21%. For both shots Z2604 and Z2605, the jet mass fraction was approximately that used in Ref. [14].

A review of the experimental data for Z2560 and Z2605 in Table II readily shows that the addition of a central jet provides only a slight improvement if the outer-to-inner shell mass ratio is 1:1.6.

The K-shell yield and peak power for these two shots are similar to that for Z2604, i.e., a shell mass ratio of 1:1 with a center jet. The same shot without a center jet, namely Z2628, had 20% less mass than Z2604, yet produced less than half the K-shell and total yields, and far less than half the peak power for both the K-shell and total. This decrease by roughly a factor of two is similar to that found by Sze *et al*.[14] on Double-EAGLE in changing from the 1:1 shell mass ratio with a central jet to the case without the jet. The pusher-stabilizer-radiator role for the triple puff may be a good description for Z2604 in comparison to Z2628, but it does not work for the first pair in Table II since Z2560 did not need a central jet to radiate as well as Z2605 with a central jet. It may be that 1:1.6 shell mass ratio is stable[10] and leads to a high yield with or without a central jet (Z2560 vs Z2605), while the 1:1 mass ratio is unstable and the addition of a massive central jet acts to stabilize the stagnation[11] and produce a high yield (Z2628 vs Z2604). Or it may be that Z2628 had too low a mass, imploded too early, and did not take advantage of the maximum current on the Z generator. In this case a larger mass would improve the K-shell yield, but how would the power behave?

The present paper aims to address these questions using the numerical simulation tool Mach2-TCRE. The magneto-hydrodynamics, non-LTE atomic physics, and radiation transport in the simulations are briefly described in the next section, as well as the circuit model for the refurbished Z generator that is coupled to the MHD. Section III describes the initial *r*-*z* gas density profile used for each separate shot in Table II. Section IV describes the simulation results. The gross properties from the simulations, such as total yield, peak total power, K-shell yield, and K-shell power are listed within parentheses in Table II. Also in this section we present simulations of Ar gas puffs with the same tailored density profile as shot Z2628 but with different total masses. The trend in the yield and powers as a function of total mass load indicate that, for Ar gas puffs on the Z generator, the mass controls the yield and the central jet enhances the peak power.

II. THE SIMULATION CODE

To model the non-linear, time-dependent evolution of an imploding Z-pinch, a resistive MHD simulation model that includes non-LTE radiation is essential. For this purpose, a modified form of the Arbitrary- Lagrangian–Eulerian (ALE) resistive MHD simulation code Mach2 is used. [18] The algorithm used therein propagates three components of the velocity, three components of the magnetic field along with the mass density in a cylindrical *r-z* geometry and azimuthal symmetry. It has been widely used to simulate a variety of plasma configurations including: field reversed magnetic fusion;[19] plasma opening switches;[20] plasma thrusters[21], galaxy clusters[22]; as well as Z-pinch physics.[23] The simulation is time-advanced in an implicit fashion without generating numerical instabilities.

To model the radiation, a computationally efficient and reasonably accurate algorithm to account for the non-LTE ionization dynamics including opacity, and non-local transport of radiation has been employed. These effects are crucial for modeling the atomic populations of high-temperature, K-shell emitting plasmas. A self-consistent equation of state is employed with a Tabular Collisional-Radiative Equilibrium (TCRE) data base model.[24] In the TCRE model, a table lookup is executed for equation of state parameters by matching them to a corresponding table entry at each plasma zone. Every table entry is characterized by three parameters: (i) specific internal energy (electron thermal plus excitation/ionization); (ii) ion density; and (iii) opacity of the dominant emission line from each populated ionization stage given the internal energy and ion density. Using these three parameters from the MHD solution and radiation transport, the radiative powers, average charge, electron temperature, etc. are then interpolated over the 3D table. The basis of the TCRE method is explained in detail in Ref. [24]. The radiation transport is calculated in three dimensional cylindrical geometry obtained from

azimuthal symmetry of the *r*-*z* computational plane.[25] The probability-of-escape formalism provides approximate solutions of the radiative transfer equation for the spectral line transport.[26] This method is very efficient and much faster than a full transport calculation. The TCRE table enables simulations in cylindrical geometry either with a local, on-the-spot approximation (OTS) or non-local models using a probability-of-escape. In the OTS approximation, if a photon is absorbed anywhere in the plasma then it is assumed to be absorbed in the emitting zone. Though the transport is calculated throughout the plasma, the OTS approximation greatly reduces the computational time needed for radiation transport because the opacity of the zones through which a photon traverses is summed. We have used the OTS approximation for all simulations presented in this paper.

MACH2-TCRE was implemented in 2D cylindrical geometry with azimuthal symmetry, azimuthal magnetic field, and in-plane (*r*, *z*) velocities. We used classical Braginskii[27] transport coefficients for the resistivity, ion and electron thermal conductivities, and ion and electron thermal equilibration. In the radial direction, a radially inward moving quasi-Lagrangian, adaptive grid is used to increase grid resolution near stagnation. The uniformly distributed grid is compressed from an initial 5.0-cm radius to ~2.0-cm radius at stagnation. This improves the resolution near the stagnation time when the K-shell radiation maximizes. There are 128 radial and 128 axial grid points used in the calculations. It must be noted that the 2D cylindrical radiation-MHD model is not valid once the pinch breaks up after stagnation and hence results from the simulations after stagnation are not discussed.

A circuit model for the current flow is also essential for self-consistently simulating a Z-pinch implosion. The current from the pulsed power machine that reaches the load controls the implosion physics and radiative output for radiation sources. A transmission line circuit model for driving 3D resistive MHD wire array Z-pinch calculations was outlined in Jennings *et al*., [28] and utilized in the code GORGON. An equivalent, lumped circuit model for the Z machine was developed by Thornhill *et*

al.[29] that consists of a voltage driver in series with a resistor and inductor. We note that the driver voltage in Ref. [29] is not the same as the stack voltage. The driver voltage is further back in the generator and should be transit time isolated from temporal changes in the load impedance. The inductor is split into several sections by two shunts to ground. The shunt $R_{MITL}(t)$ represents the time-dependent current losses in the magnetically insulated transmission line (MITL) region. The shunt $R_{feed}(t)$ is a time-dependent element for modeling current losses downstream from the posthole convolute at the beginning of the final feed. For these shunts the time variation is taken as

$$R_{MITL}(t) = R_{feed}(t) = \begin{cases} 5\ \Omega, \text{ for } t \le t_o = 115 \text{ ns} \\ 0.2 + (5 - 0.2)\exp[-(t - t_o)/4 \text{ ns}]\ \Omega, \text{ for } t > t_o \end{cases} \quad (1)$$

The time t_o is measured from the beginning of the driver voltage. The total current that flows along several separate MITLs is denoted by I_{MITL}. The current measured downstream of the posthole convolute and flowing through the final feed is I_{feed}. I_{load} is the current that reaches the gas-puff plasma. This is the driving current of the pinch but has proved to be a challenge to measure. The shunt parameters in Eq. (1) were determined by matching the measured range of I_{MITL} and I_{feed}, as well as the radiation properties, for the three Ar shots in Ref. [9].

For the (r, z) geometry of the Mach2-TCRE code with only an azimuthal magnetic field (B_φ), the load voltage (V_{load}) in the circuit equation for the Z generator is derived from Faraday's law by an areal integration over the load region out to the fixed return current radius (r_w):

$$\begin{aligned} V_{load} &= \int_0^\ell dz E_z(r=0,z,t) + \frac{d}{dt}\left(\frac{1}{c}\int_0^\ell dz \int_0^{r_w} dr B_\varphi\right) \\ &= \int_0^\ell dz \eta_\perp J_z(r=0,z,t) + \frac{d}{dt}\left(\frac{1}{c}\int_0^\ell dz \int_0^{r_g(t)} dr B_\varphi\right) + \frac{d}{dt}\left[\frac{2\ell I_{load}}{c^2}\ln\left(\frac{r_w}{r_g(t)}\right)\right] \end{aligned} \quad (2)$$

where ℓ is the axial height of the pinch, $\eta_\perp$ is the perpendicular Spitzer resistivity, and $r_g(t)$ is the outer radius of the inward moving computational grid. The first term in the second line arises because there is no motional electric field along the z-axis. The middle term is the magnetic flux in the computational grid, and the third term is the magnetic flux in the vacuum region between the return current radius and the outer edge of the grid. Together the last two terms are the inductive load on the circuit. As the pinch implodes, the edge of the dense plasma, and hence the location of the magnetic piston, is not at a single radial position but becomes irregular due to the MRT instability. An artificial resistivity is used in the regions where the mass density drops below a fixed value to force the current density to vanish and the magnetic field to vary inversely with the radius in such regions.

III. INITIAL DENSITY PROFILE

Nonlinear evolution of the Z-pinch implosion dynamics depends on the initial density distribution and mass load. Simulations of neon on the generator at Weizmann Institute of Science have shown that knowledge of the initial gas density profile can be essential for matching the experimental data of the pinch.[30] Simulations presented herein were initialized using smoothed two-dimensional interferometry data from a Mach-Zehnder imaging interferometer.[31] A two-step smoothing was performed because the measured interferometry data had spurious fluctuations in density near $r = 0$ due to numerical noise in Abel inversion. First, a graphical user interface was developed to manually eliminate some of the non-physical, local variations. In addition to pruning of the data, a multi-dimensional smoothing filter that performs averaging of nearest neighbors was also implemented on a single pass throughout the r-z data plane of density.[29] It is necessary to prune and smooth the data to prevent numerical noise from introducing spurious seeds to the MRT instability. The resultant data for the initial mass density $\rho(r,z,t=0)$ was finally interpolated onto a finer grid suitable for our numerical simulations. Density profile lineouts are shown in Fig. 1 (a-d) at three different axial heights for each of the four shots in Table II. Note that shots Z2560 and Z2628 with only the double shells have the same profile at r > 2.5 cm, but the change in density from the peak of the inner shell to $r = 2$ cm is much greater for Z2560 than for Z2628. The density profile for the inner shell in Z2560 is analogous to the profile proposed in Velikovich *et al*.[10] to limit MRT disruption. For the two shots with a central jet (Z2605 and Z2604), the gap between the inner shell and the jet fills and the density profile becomes more monotonic as one looks downstream of the nozzle exit. In this region the density profiles are approaching the ideal distribution suggested by Hammer *et al*.[11] to limit MRT disruption. Recently Jennings *et al*.[32] showed from hydrodynamic computations that the nozzle opening for the inner shell could be designed to produce a ramped profile that more closer resembles the ideal distribution of Hammer *et al*.

IV. SIMULATION RESULTS

Simulations were performed for the four shots listed in Table II using the Mach2-TCRE radiation-MHD code and the circuit model described in Section II and the smoothed (r, z) initial density profiles from Section III. The calculated gross radiation properties have been listed in Table II within parentheses: total (Y_{tot}) and K-shell (Y_K) yield; peak total power (P_{tot}), P_K; and Δt_K. The simulation results do not reproduce the data precisely, but do follow the general trends: (i) for both the 1:1.6 and 1:1 shell mass ratios, P_{tot} and P_K increase when a central jet is added to the double-shell configuration; and (ii) the 1:1 shell mass ratio without a central jet severely underperforms in all four of the radiation properties. More details of the simulations for the four Ar shots are shown in Fig.2. First, we compare the calculated K-shell pulse with the experimental data. For Z2560 and Z2604 the calculated pulse width is slightly broader and the peak power less than the data, while for Z2605 the calculated width matches the data but the peak power is too large. The peak of the K-shell power occurs between 160 ns and 190 ns from the start for all the simulations. The experimental pulse widths are ≤ 10 ns, except for Z2628 where the low value of P_K and the broad tail (~30 ns) are captured in the simulation.

Figure 2 also presents the calculated MITL, feed, and load currents for the four Ar shots. As mentioned in the Introduction, Z2560 was one of three repeated shots (Z2559 – Z2561) that had the same nozzle, plenum pressures, and the total mass load.[9] The measured range for the MITL and feed currents covering these three shots is presented as shaded bands in Fig.2(a). For the remaining shots the measured stack current is shown as a dotted line as well as a shaded region for the feed current. The shaded grey regions represent the minimum and maximum values recorded by several B-dots arranged azimuthally around the feed to the gas-puff load. We have interpreted this B-dot data as indicative of the feed current, not I_{load} in the plasma region. Clearly a single circuit model with fixed current losses does not accurately describe each shot. A delay of the turn-on time for the current loss by a few ns in Eq. (1)

would give better agreement for the MITL and feed current in Z2605 and Z2604. The results using a single model calibrated to one shot (Z2560) indicate the accuracy one can expect when predictive calculations are required. The time in these plots is a simulation time wherein the equivalent voltage for the driver starts at $t = 0$. The separation of the MITL, feed, and load currents begins when the shunts in Eq. (1) are initiated. The MITL or stack currents are fairly independent of the gas-puff configuration and the linear mass load because the rapid decrease in the shunt resistance isolates the driver from the load. Notice that the calculated I_{load} at peak power (~9MA) in Z2628 is similar to the corresponding values for Z2604 and Z2560. This indicates that the magnetic energy at the boundary is nearly the same for all shots. Furthermore, Z2628, which has a linear load mass of m_ℓ = 0.77 mg/cm ± 10% was the lowest linear load mass attempted. But the load mass was only 23% lower than Z2604 and Z2560, yet the K-shell yield observed dropped by more than a factor of two.

Is the poor yield performance of Z2628 solely attributable to a poor matching of the load to the generator? The simple 1D, snowplow scaling relation connecting the load conditions to the generator is

$$M_o r_o^2 \propto \Delta L I_{pk}^2 t_{imp}^2 \tag{3}$$

where M_o is the total load mass, r_o is the initial outer radius of the gas puff (= 4 cm), ΔL is the change in load inductance during the implosion [$= (2\ell / c^2)\ln(r_o / r_f)$, where ℓ is the pinch length and r_f is the final radius at stagnation], I_{pk} is the peak load current, and t_{imp} is the implosion time measured between the extrapolation of the linear portion of the current rise back to the time axis and the time of P_K. From Fig. 2 the peak load current is 15 MA for each of the four simulations. Suppose ΔL is also the same. For the two configurations without a central jet, the experimental profiles in Fig.2 give t_{imp} ~109 ns for Z2560 and ~99 ns for Z2628. For these two shots, the square of the ratio of the implosion times is nearly the ratio of the total mass loads (1/0.77) = 1.3. Thus we want to consider how the radiation properties

would change if the mass of Z2628 were different but with the same 1:1 outer-to-inner shell mass ratio and no central jet.

The load mass of Z2628 was varied by multiplying its initial density profile $\rho(r,z,t=0)$ by a constant factor such that the linear load mass (m_ℓ) covered the range 0.6 to 1.35 mg/cm. In Fig. 3(a), the calculated Y_{tot} and Y_K are presented as a function of m_ℓ. The points with circles and error bars are the experimental values for Z2628 and Z2604. For example, the error bar for Z2604 indicates a mass of m_ℓ=1.0 mg/cm with a 10% uncertainty and a 9% uncertainty in P_K. As the linear load mass was increased from 0.76 mg/cm, the yields Y_{tot} and Y_K likewise increase and reach the yield values for Z2604 at m_ℓ~1.05 mg/cm. Hereinafter we denote the simulated shot with the density profile of Z2628, but a total linear load mass of 1.05 mg/cm, as Z2628*. Though not plotted, one can see from Table II that Z2628* also has Y_{tot} and Y_K similar to Z2560 and Z2605. Fig. 3(a) also indicates that a load mass of ~1.2 mg/cm would be optimal for obtaining the greatest amount of K-shell yield for this configuration, assuming that the circuit model of Section II is not changed by the higher mass loading. In Fig. 4(b), the calculated values of P_{tot} and P_K are presented as a function of m_ℓ. Here we see a contrary result to that of the yields, namely the simulated peak powers cannot match the observed values for Z2604 for any mass loading. The result for the simulation Z2628* is indicated on Fig. 4(b) using a black asterisk. The K-shell power obtained in simulations of Z2628 was only 4.7 TW. For Z2628* the computed powers P_{tot} and P_K are 24 TW and 12 TW, respectively, but much lower than the powers in Z2604. We find that the double-shell configuration with a higher load mass (Z2628*) can match the yields of the double shell plus center jet (Z2604), but not the powers.

Because Y_K for Z2628* is close to that for Z2604, the P_K is less, the pulse width for Z2628* is much broader than in Z2604. The broadening of the pulse was also examined for other values of load

mass. The K-shell radiation pulse width became wider as the linear load mass was decreased from 1.0 to 0.56 mg/cm, indicating that the pulse width is sensitive to the load mass. In simulations with lower load mass, the plasma imploded earlier as indicated by an earlier time for P_K.

We now examine in more detail the implosion dynamics of the poorly performing shot Z2628. The temporal evolution of the mass density and K-shell radiative power density are shown in Fig. 4. Each row is at a different time denoted relative to the time of P_K. Between $t = -162$ ns [Fig.4(a)] to $t = -61$ ns [Fig. 4(b)], the mass of the outer shell is ionized and swept into a thin snowplow, while the inner shell remains largely unaffected. Between $t = -61$ ns to $t = -22$ ns, more matter is ionized, heated and swept into the snowplow. By about $t = -11$ ns, the two shells have been completely swept into the snowplow and the temperature continues to increase, giving rise to a foot in the K-shell radiation pulse. At this time the outer edge is developing non-linear MRT fingers. By $t = -6$ ns a hot, radiating spot is formed near the top that travels down along the axis (zippering). Through the stagnation stage the P_K ~4.7 TW is produced, releasing about 155 kJ of K-shell radiation energy. Notice that the neither the density nor the K-shell radiation is distributed uniformly along the z-axis. We find that zippering along the z-axis lasts ~10 ns and thus is not the cause of the long ~30 ns K-shell pulse width.

The low P_K for Z2628 and Z2628* could arise from the MRT instability during the implosion dynamics. The bubble and spike structure of the implosion has been proposed[33] as one mechanism by which MRT instability influences the width of the radiation pulse at stagnation. In this model, the pinch begins to radiate when the leading bubble first reaches the axis, and it continues to radiate as the remaining mass in the spikes and other parts of the shell also arrive on axis. Consequently, the spike-to-bubble distance may be used as a measure of broadening of the radiation pulse. We use the distribution of the current to reveal the bubble and spike structure of the pinches. In Fig. 5, color contours of the current ($= crB_\varphi / 2$) are plotted on the (r, z) plane at the time of P_K for simulations of the shots in Table

II as well as Z2628*. Bubbles and spikes are present in all cases. Z2628 has the largest bubble to spike distance in the set. Consequently, the K-shell pulse of Z2628 is expected to be the broadest. On the other hand, Z2605 has the smallest bubbles and the weakest spikes would be expected to radiate in a shorter pulse. The solid blue line in each of the subfigures is the boundary at which the current is half its value at the right edge. The skin depth for the current distribution follows this boundary and is much shorter than the scale of the MRT spikes and bubbles. The geometric variation of this boundary, which locates the magnetic piston, with segments of large and small-scale curvature, means that the simple 1D formula used in Eqn. (3) for the pinch inductance is not realistic. The simulation code computes the inductive load including the undulating magnetic piston according to Eqn. (2) and the following discussion.

Figure 5 suggests that the material of Z2628 is spread over a large volume at the time of P_K compared to the other shots because the boundary of the current sheath encompasses a larger volume. In Fig. 6(a) the normalized integral of the mass at the initial time is illustrated. All profiles have fractional mass of unity by the r = 5 cm boundary. The initial normalized distributions for the two shots with a central jet (Z2604 and Z2605) rise the fastest near the origin, and that for Z2560, with the 1:1.6 shell mass ratio catches up by $r \sim 2$ cm. For the remaining two cases, Z2628 and Z2628*, the normalized distributions rise more slowly and does not reach a similar mass concentration until nearly 4 cm. Effectively the initial center-of-mass radius is larger for Z2628 and Z2628* (r_{CM} ~2.5 cm) than for Z2560 (r_{CM} ~2.25 cm) and for the other two shots with a central jet ($r_{CM} \leq 2$ cm). These initial normalized mass distributions appear to have a significant impact by the time of stagnation, as illustrated in Fig. 6(b). The normalized mass distributions for Z2560, Z2605, and Z2604 are far more concentrated toward the axis than Z2628 and Z2628*. Not only does Z2628 have the smallest linear load mass in the set, it also has the least concentration of mass close to the axis near stagnation. In other words, for Z2628 a significant fraction of mass is left at large radius at the time of P_K. This also implies that Z2628

has a larger effective radius than Z2604 at stagnation. For example in Z2604, about 90% of the mass is located within 0.8 cm of the axis with an average mass density of ~0.4 mg/cm^3, while in Z2628 the same percentage of mass is located within a radius of ~1.4 cm with an average mass density four times less.

The radial distribution of the axially averaged mass density near the axis correlates with the peak K-shell power. Figure 7 shows this mass density versus radius for all five shots under consideration at the time of P_K. The averaged mass density for Z2628 is ~1 mg/cm^3, varies slowly, and has the smallest P_K. The simulation Z2628* has the second lowest density of ~2 mg/cm^3 and the second lowest P_K. Finally Z2605 has the highest density and the largest simulated P_K. Thus for the initial density profiles examined for these shots on the Z generator, those shots with a simulated high P_K have a simulated high density on axis at peak power.

The low values of Y_{tot} and Y_K for Z2628 are attributable to the high electron temperature (T_e) but low mass in the K-shell ionization stage. These properties can be seen by comparing the mass in various ionization stages for each simulated shot at the time of stagnation as listed in Table III. The ratio of the H-like to the He-like population increases with T_e and from the table we see that Z2628 has the highest H-like/He-like ratio compared to the other simulated experiments. In addition Z2628 also has the lowest mass in the K-shell ionization stage. Here m_K is the sum of the linear mass in the He-like, H-like, and stripped stages. For Z2628* the H-like/He-like is smaller and the linear mass in the K-shell is larger than for Z2628. These values for Z2628* are closer to those for the shots Z2560, Z2605, and Z2604. Table III also lists the center-of-mass radius (r_{CM}), the inductive radius (r_{ind}) and the radius (r_K) of the K-shell emitting region from the simulations. The inductive radius is calculated from the formula,

$$\ln\left(\frac{r_o}{r_{ind}}\right) = \frac{c^2}{\ell I^2} E_B \qquad (4)$$

where E_B is the magnetic energy. The radius r_{ind} is the effective location of the magnetic piston that drives the implosion. The importance of this piston can be assessed by comparing r_{CM} and r_{ind} as a measure of the plasma confined by the magnetic piston. The case $r_{ind} < r_{CM}$, implies a significant mass is within the piston. Note that $r_{ind} < r_{CM}$ for the shots that yielded low peak K-shell power (i.e. Z2628 and Z2628*), but $r_{ind} \sim r_{CM}$ for others. Consequently, $r_{ind} < r_{CM}$ is also consistent with a broader mass distribution and a broader K-shell radiation pulse. Note, in a 0D snowplow model, where MRT is absent, $r_{ind} > r_{CM}$. The radius r_K is defined as the axially averaged radius where the K-shell power decreases to 90% of the total P_K. In all cases $r_{CM} \geq r_K$. The mass inside of r_K from Fig. 6(b) for each simulation is close but not exactly equal to m_K in Table III. This feature arises from the multi-dimensional distribution of the K-shell emitting mass.

The next column of Table III lists the computed mass weighted, average electron temperature within r_K, $\langle T_e \rangle_K = \int dz \int_0^{r_K} T_e \rho 2\pi r dr / \int dz \int_0^{r_K} \rho 2\pi r dr$. One can see that $\langle T_e \rangle_K$ varies in the same manner with shot number as the H-like/He-like ratio in column six. Furthermore, $\langle T_e \rangle_K$ varies inversely with the mass density at stagnation as shown in Fig. 7. This last inverse correlation agrees with the analysis of the spectral data for the experimental shots of Table I presented in Ref. [17].

Figures 5, 6, and 7 and Table III present plasma conditions at the time of P_K. We lastly examine the energy coupled from the current driver throughout the radiation pulse. From the simulations we find that the coupling is primarily through the Maxwell stress term in the momentum equation rather than resistive heating. Specifically the computed coupled energy is given by

$$E_{J\times B}(t) = \int_0^t dt \int dz \int dr 2\pi r \left(\frac{\boldsymbol{v}}{c} \cdot \boldsymbol{J} \times \boldsymbol{B}\right) \quad (5)$$

where υ is the plasma velocity and c is the speed of light. This calculated coupled energy and with the calculated K-shell radiation pulse is presented in Fig.8 for all of our simulations. As the coupled energy increases, the plasma begins to emit K-shell radiation. The undulations in $E_{J\times B}$ are indicative of the interactions of the imploding plasma with the different shells, and in the case of Z2604 with the central jet. During stagnation the peak K-shell power and pulse width is related to the slope of $E_{J\times B}$, which is the power coupled to the plasma. For example, the slope of $E_{J\times B}$ for shot Z2605 is the largest and also has the largest K-shell power and the shortest pulse width. The opposite case holds for Z2628. For this shot $E_{J\times B}$ flattens and decreases slightly during much of the K-shell pulse. From (4) this can only occur if the velocity is small and changes sign, i.e., the plasma sheath stops imploding and rebounds. Thus Z2628 undergoes a bounce around the time of P_K that halts the coupled power and limits any further increase in P_K from value of ~4.7 TW.

The penultimate column of Table III lists $E_{J\times B}$ at the last time displayed in Fig.8. If $E_{J\times B}$ is shared among all the ions in the load and then divided by $E_{\min}$ the result is a theoretical η*-parameter and is listed in the last column of Table II. $E_{\min}$ is the minimum energy per ion needed to produce both ionization into the K-shell and strong excitation of the He-like emission lines. For Ar, $E_{\min}$ = 40keV per ion.[34],[35] Values of η* should be ≥ 2 in order to overcome radiation losses during implosion and here they are all similar and ~4. The variation in Y_K and P_K in both the shot data and the simulations indicate that η* ~2 is a necessary but not sufficient condition for optimal yield and power.

V. SUMMARY

Advanced nozzles producing tailored density profiles formed by a double shell and a central jet have been used in gas-puff Z-pinches for K-shell radiation sources for over a decade. Interest in a central jet arose from the large diameter (12 cm) Ar experiments on the DE and DQ generators that produced a factor of > 2 increase in Y_K and P_K with a central jet compared to just a double shell with a 1:1 shell mass ratio (Table I). The triple nozzle platform was described as a "pusher-stabilizer-radiator" for the outer shell, inner shell, and central jet.[14] The inner shell purportedly acted to stabilize the implosion against the MRT instability. Recent Ar experiments with an 8 cm diameter double shell were performed on the pulsed power Z generator at SNL to investigate the role of the central jet on the radiation source properties.[17] One pair of these experiments (Z2560 and Z2605) used 1:1.6 for the mass ratio of outer-to-inner shell, and the second pair (Z2628 and Z2604) used 1:1 for the same ratio. In each pair, one of the shots had a central jet (Z2605 or Z2604). In the present paper simulations of the Z experiments were presented using the 2D (r, z) radiation-MHD code Mach2-TCRE with the measured density profiles (Fig. 1) and the same circuit model for all the runs (Fig. 2). Table II lists the data for four shots and compares the experimental and simulated results for the total and K-shell yields, corresponding powers, and pulse widths. The observed trends in the radiation properties among the four shots are reproduced by the simulations.

For the Z experiments and the present simulations the two Ar gas puffs with a 1:1.6 shell mass ratio did not exhibit the same increase by a factor of two in K-shell yield seen in earlier longer pulse experiments on Double Eagle and Decade Quad that were designed on the pusher-stabilizer-radiator paradigm. Adding a central jet barely increased Y_K (same for the simulations) and there was a ~12% increase in P_K (64% increase for the simulations). The case for the two shots with a 1:1 shell mass ratio

is more complex. Adding a central jet (Z2604) increased Y_K the P_K by a factor of 2.5 and 5.4, respectively in experiments, and by 3.1 and 5.3, respectively in simulations, compared to Z2628. One caveat though was that Z2628 had a total linear mass of only 0.77 mg/cm, ~23% less mass than Z2604, and suggesting that it was not properly matched to the Z driver, as evidenced by the slightly shorter implosion time in Fig. 2(d) compared to Fig. 2(c). We examined this possibility by modeling hypothetical shots of the same 1:1 density profile as Z2628 but with a larger total mass (Fig.3). It was assumed that the current loss properties of our Z circuit model did not change. We found that if the mass of Z2628 were increased to 1.05 mg/cm (= Z2628*), then its K-shell yield could match that of Z2604 and the other experimental shots. On the other hand, no reasonable mass increase could match the peak K-shell power of Z2604 with a central jet and the same outer-to-inner shell mass ratio.

Based on these results it appears that the pusher-stabilizer-radiator concept, as implemented here by having more mass on axis for these 8 cm diameter nozzles, applies to the peak K-shell power for the 1:1 shell mass configurations but less so for the inherently more stable 1:1.6 shell mass configuration. In the 1:1.6 shell mass ratio Z experiments the pusher-stabilizer-radiator concept did not result in the same increase by a factor of two in K-shell yield observed in the Double Eagle and Decade Quad long pulse experiments. This is not a surprising result since the 1:1.6 mass ratio without central jet configuration experiment converted ~30% of the machine coupled energy into K-shell X rays. This conversion efficiency is typical of the maximum value calculated in idealized (stable) 1D argon simulations for loads that have enough mass and coupled energy to be in the so called efficient scaling regime. Such a high conversion efficiency also indicates that the load is sufficiently stable to produce maximal K-shell emission. An increase of a factor of two beyond ~30% due to the further stabilizing influence provided by the addition of a central jet would have been a substantial accomplishment. Conversely, the Double Eagle and Decade Quad experiments had lower η* values and lower masses such that it is likely they

were performed in an inefficient scaling regime. Idealized 1D calculations in this range show that K-shell conversion efficiencies are < 20% and that the K-shell powers and yields increase as the square of coupled energy.[35] In other words, K-shell yields in the inefficient regime are more sensitive to load mass and design and other considerations that effect energy coupling than are experiments performed in the efficient scaling regime.

All of the four simulated shots in Table II and Z2628* show significant MRT structure by the time of stagnation (Fig. 5), though more so for Z2628. The major difference of Z2628 from the other experimental shots is the lack of compression at stagnation, as evidenced in Fig.6 (b). This feature leads to the lowest central density at stagnation. The lower density leads to less radiative cooling which leads to hotter plasmas that are more difficult to compress. Actually we find that the simulated central density at stagnation from Fig. 7 is correlated with the calculated P_K in Table II. Table II and Table III show that the weak compression of Z2628 arises because of the reduced radiative cooling. Since the local cooling power $\propto n^2$, the plasma is hotter and more difficult to compress in this simulation than in all the others This case has the largest H-like/He-like ratio and the highest K-shell averaged electron temperature $\langle T_e \rangle_K$. Hence Z2628 is over ionized for a good K-shell source. On the other hand, because Z2628 had the lowest mass loading, it also has the least mass ionized into the K-shell. These two features, excessive temperature and low K-shell mass, explain the low yield of Z2628. The case for Z2628* is somewhat better: it has a lower $\langle T_e \rangle_K$ and more mass in the K-shell. As a result Y_K is larger for Z2628* than for Z2628, but because the compression in Fig. 6(b) only slightly improves from Z2628, the P_K for double-shell loads on the Z generator with a 1:1 mass ratio cannot attain the higher power values obtained with a central jet. The high temperature in Z2628 causes the plasma to bounce, which in turn limits the coupled energy $E_{J\times B}$ during much of the K-shell pulse as shown in Fig. 8. On

the other hand, $E_{J\times B}$ for those loads with a central jet (Z2604 and Z2605) continues to increase during stagnation as the pinch continues to compress.

The experimental shots and simulations listed in Tables I and II along with Fig. 2 show that the shape of the Ar K-shell radiation shape depends on the initial density profile in the gas puff. If the mass ratio of the outer-to-inner shell is 1:1.6 then the pulse has a narrow width and attains a high peak power, whether or not there is a central jet. For a mass ratio of 1:1, a narrow pulse is obtained only with a central jet. Additional simulations for the 1:1 ratio showed that even at a larger total mass, the K shell pulse is broad. For the 1:1.6 case in Table II we found in the simulations that the peak K-shell pulse was much larger with central jet (41 TW) than without (25 TW), while the experiment gave only a moderate increase (32 vs 28.5 TW). There are experiments, however, that show a large improvement in the output with a larger inner-to-outer mass ratio. One of the 12 cm diameter Ar shots with a central jet described in Sze *et al* [14] had a much greater outer-to-inner mass ratio, namely 1:4.2,[13] and it had a 24% larger peak K-shell power than the 1:1 shot with a central jet. An extreme example, though not for Ar, is the factor of ten increase in the neutron yield found by Klir et al.[36] when a low mass liner from plasma guns (5μg/cm) at a large diameter (35 cm) was added to a deuterium gas puff of ~100 μg/cm and 8 cm diameter. It remains to be investigated, both experimentally and computationally, whether Ar gas puffs of 8 cm diameter with a central jet and a larger ratio than 1:1.6 for the outer-to-inner shell mass ratio will further increase the peak K-shell power and/or yield.

ACKNOWLEDGEMENTS

Work by NRL authors was supported by DOE/NNSA. John Giuliani would like to thank Robert Commisso of NRL for fruitful discussions on the analysis and Niansheng Qi of L-3, ATI and Christine Coverdale of SNL for correspondence on previous experimental data. Sandia National Laboratories is a multi-program laboratory managed and operated by Sandia Corporation, a wholly owned subsidiary of Lockheed Martin Corporation, for the U.S. Department of Energy's National Nuclear Security Administration under contract DE-AC04-94AL85000.

REFERENCES

[1] J. L. Giuliani and R. J. Commisso, "A Review of the Gas-Puff Z-Pinch as an X-Ray and Neutron Source", IEEE Trans. Plasma Sci., vol. 43, no. 8, pp.2385–2453, 2015.

[2] H. Sze, P. L. Coleman, J. Banister, B. H. Failor, A. Fisher, J. S. Levine, Y. Song, E. M. Waisman, J. P. Apruzese, R. W. Clark, J. Davis, D. Mosher, J. W. Thornhill, A. L. Velikovich, B. V. Weber, C. A. Coverdale, C. Deeney, T. L. Gilliland, J. McGurn, R. B. Spielman, K. W. Struve, W. A. Stygar, and D. Bell, "Efficient argon K-shell radiation from a Z-pinch at currents >15 MA", *Phys. Plasmas*, vol. 8, no.7, pp. 3135–3138, Jul. 2001.

[3] Y. Song et al., "Valve and nozzle design for injecting a shell-on shell gas-puff load into a Z-pinch," Rev. Sci. Instrum., vol. 71, no. 8, pp. 3080–3084, Aug. 2000.

[4] C. A. Coverdale, C. Deeney, B. Jones, J. W. Thornhill, K. G. Whitney, A. L. Velikovich, R.W. Clark, Y. K. Chong, J. P. Apruzese, J. Davis, and P. P. LePell, "Scaling of K-shell emission from Z-pinches: Z to ZR", IEEE Trans. Plasma Sci., vol. 35, no. 3, pp. 582–591, Jun. 2007.

[5] J. P. Apruzese, J. L. Giuliani, J. W. Thornhill, C. A. Coverdale, B. Jones, and D. J. Ampleford, "Analysis of spatially resolved Z-pinch spectra to investigate the nature of 'bright spots'", Phys. Plasmas, vol. 20, no. 10, pp. 022707-1–022701-10, 2013.

[6] M. Krishnan , K. W. Elliott , R. E. Madden , P. L. Coleman , J. R. Thompson , A. Bixler , D. C. Lamppa , J. L. McKenney , T. Strizic , D. Johnson , O. Johns , M. P. Vigil , B. Jones , D. J. Ampleford , M. E. Savage , M. E. Cuneo , and M. C. Jones, "Architecture, implementation, and testing of a multiple-shell gas injection system for high current implosions on the Z accelerator", Rev. Sci. Instrum., vol. 84, no. 6, pp. 063504-1–063504-19, 2013.

[7] J. W. Thornhill, J. L. Giuliani, Y. K. Chong, A. L. Velikovich, A. Dasgupta, J. P. Apruzese, B. Jones, D. J. Ampleford, C. A. Coverdale, C. A. Jennings, E. M. Waisman, D. C. Lamppa, J. L. McKenney, M. E. Cuneo, M. Krishnan, P. L. Coleman, R. E. Madden, and K. W. Elliott, "Two-dimensional radiation MHD modeling assessment of designs for Argon gas puff distributions for future experiments on the refurbished Z machine", *High Energy Density Phys*., vol. 8, pp.197–208, 2012.

[8] B. Jones, C. A. Jennings, D. C. Lamppa, S. B. Hansen, A. J. Harvey-Thompson, D. J. Ampleford, M. E. Cuneo, T. Strizic, D. Johnson, M. C. Jones, N. W. Moore, T. M. Flanagan, J. L. McKenney, E. M. Waisman, C. A. Coverdale, M. Krishnan, P. L. Coleman, K. Wilson Elliott, R. E. Madden, J. Thompson, A. Bixler, J. W. Thornhill, J. L. Giuliani, Y. K. Chong, A. L.

Velikovich, A. Dasgupta, and John P. Apruzese, "A renewed capability for gas puff science on Sandia's Z machine", IEEE Trans. Plasma Sci., vol. 42, no. 5, pp. 1145–1152, May 2014.

[9] B. Jones, J. P. Apruzese, A. J. Harvey-Thompson, D. J. Ampleford, C. A. Jennings, S. B. Hansen, N. W. Moore, D. C. Lamppa, D. Johnson, M. C. Jones, E. M. Waisman, C. A. Coverdale, M. E. Cuneo, G. A. Rochau, J. L. Giuliani, J. W. Thornhill, N. D. Ouart, Y. K. Chong, A. L. Velikovich, A. Dasgupta, M. Krishnan, and P. L. Coleman, "The effect of gradients at stagnation on K-shell X-ray yield in high-current Ar gas puff implosions", Phys. Plasmas,, vol. 22, no. 2, pp. 020706-1–020706-5, Feb. 2015.

[10] A. L. Velikovich, F. L. Cochran, and J. Davis, "Suppression of Rayleigh-Taylor instability in Z-pinch loads with tailored density profiles", *Phys. Rev. Lett*., vol.77, no.5, pp.853–856, Jul. 1996.

[11] J. H. Hammer, J. L. Eddleman, P. T. Springer , M. Tabak , A. Toor , K. L. Wong , G. B. Zimmerman , C. Deeney , R. Humphreys , T. J. Nash , T. W. L. Sanford , R. B. Spielman , and J. S. De Groot, "Two dimensional radiation magnetohydrodynamic simulations of SATURN imploding Z-pinches", *Phys. Plasmas*, vol. 3, no. 5, pp. 2063–2069, May 1996.

[12] J. S. Levine, J. W. Banister, B. H. Failor, N. Qi, Y. Song, H. M. Sze, and A. Fisher, "Long implosion time (240 ns) Z-pinch experiments with a large diameter (12 cm) double-shell nozzle", Phys. Plasmas, vol. 11, no. 5, pp. 2054–2059, May 2004.

[13] J. S. Levine, J. W. Banister, B. H. Failor, N. Qi, H. M. Sze, A. L. Velikovich, R. J. Commisso, J. Davis, and D. Lojewski, "Implosion dynamics and radiative characteristics of a high yield structured gas puff load", Phys. Plasmas, vol. 13, no.8, pp. 082702-1–082702-11, 2006.

[14] H. Sze, J. Banister, B. H. Failor, J. S. Levine, N. Qi, A. L. Velikovich, J. Davis, D. Lojewski, and P. Sincerny, "Efficient radiation production in long implosions of structured gas-puff Z-pinch loads from large initial radius", *Phys. Rev. Lett*., vol.95, pp.105001-1–105001-4, Sep. 2005.

[15] A. S. Chuvatin, L. I. Rudakov, A. L. Velikovich, J. Davis, and V. I. Oreshkin, "Heating of on-axis plasma heating for keV X-ray production with Z-pinches," IEEE Trans. Plasma Sci., vol. 33, no. 2, pp. 739–751, Apr. 2005.

[16] F. C. Young, R. J. Commisso, D. P. Murphy, J. P. Apruzese, D. Mosher, A. L. Velikovich, P. L. Coleman, J. W. Banister, B. H. Failor, J. S. Levine, N. Qi, and H. M. Sze, "Measurement and analysis of continuum radiation from a large-diameter long implosion time argon gas puff Z-pinch at 6 MA", IEEE Trans. Plasma Sci., vol. 34, no. 5, pp. 2312–2324, Oct. 2006.

[17] A. J. Harvey-Thompson, C. A. Jennings, B. Jones, D. J. Ampleford, D. C. Lamppa, C. A. Coverdale, M. E. Cuneo, S. B. Hansen, M. C. Jones, N. W. Moore, G. A. Rochau, J. P. Apruzese, J. L. Giuliani, and J. W. Thornhill, "Investigating the effect of adding an on-axis jet to Ar gas puff Z-pinches on Z", Phys. Plasmas, this issue (2015).

[18] R. E. Peterkin , M. H. Frese, and C. R. Sovinec, "Transport of magnetic flux in an arbitrary coordinate ALE code", J. Comp. Phys., vol. 140, pp. 148–171, 1998.

[19] Domonkos, M. T., Amdahl, D., Camacho, J. F., Coffey, S. K., Degnan, J. H., Delaney, R., Frese, M., Gale, D., Grabowski, T. C., Gribble, R., Intrator, T. P., McCullough, J., Montano, N., Robinson, P. R. and Wurden, G. "Applied magnetic field design for the field reversed configuration compression heating experiment", Rev. Sci. Instrum., vol. 84, p 043507, 2013.

[20] J. W. Schumer, S. B. Swanekamp, P. F. Ottinger, R. J. Commisso, B. V. Weber, D. N. Smithe, and L. D. Ludeking, "MHD-to-PIC transition for modeling of conduction and opening in a plasma opening switch", IEEE Trans. Plasma Sci., vol. 29, pp. 479-493, 2001.

[21] Pavlos G. Mikellides, Peter J. Turchi, and Norman F. Roderick. "Applied-Field Magnetoplasmadynamic Thrusters, Part 1: Numerical Simulations Using the MACH2 Code", Journal of Propulsion and Power, Vol. 16, No. 5 (2000), pp. 887-893.

[22] Mikellides, I. G., Tassis, K. and Yorke, H. W., "2D Magnetohydrodynamics simulations of induced plasma dynamics in

the near-core region of a galaxy cluster", Mon. Notices Royal Astron. Soc., vol. 410, 2602-2616, 2011.

[23] J. W. Thornhill, Y. K. Chong, J. P. Apruzese, J. Davis, R. W. Clark, J. L. Giuliani, R. E. Terry, A. L. Velikovich, R. J. Commisso, K. G. Whitney, M. H. Frese, S. D. Frese, J. S. Levine, N. Qi, H. Sze, B. H. Failor, J. W. Banister, P. L. Coleman, C. A. Coverdale, B. Jones, and C. Deeney, "One- and two-dimensional modeling of argon K-shell emission from gas-puff Z-pinch plasmas", Phys. Plasmas, vol. 14, pp. 063301-1–063301-14, 2007.

[24] J. W. Thornhill, J. P. Apruzese, J. Davis, R. W. Clark, A. L. Velikovich, J. L. Giuliani, Y. K. Chong, K. G. Whitney, C. Deeney, C. A. Coverdale, and F. L. Cochran, "An efficient tabulated collisional radiative equilibrium radiation transport model suitable for multidimensional hydrodynamics calculations", Phys. Plasmas, vol. 8, no.7, pp.3480–3489, Jul. 2001.

[25] J. P. Apruzese and J. L. Giuliani, "Multi-dimensional radiation transport for modeling axisymmetric Z-pinches: ray tracing compared to Monte Carlo solutions for a two-level atom", J. Quant. Spectros. Rad. Transfer, vol. 111 pp134–143, 2010.

[26] J. P. Apruzese, "An analytic Voigt profile escape probability approximation", J. Quant. Spectrosc. Rad. Transfer, vol. 34, no. 5, pp. 447–452, 1985.

[27] S. I. Braginskii, "Transport processes in a plasma", in Reviews of Plasma Physics, edited by M. A. Leontovich (Consultants Bureau, New York, 1965), vol. 1, pp. 205–311.

[28] C. A. Jennings, J. P. Chittenden, M. E. Cuneo, W. A. Stygar, D. J. Ampleford, E. M. Waisman, M. Jones, M. E. Savage, K. R. LeChien, and T. C. Wagoner, "Circuit model for driving three-dimensional resistive MHD wire array Z-pinch calculations", IEEE Trans. Plasma Sci., vol. 38, no. 4, pp. 529–539, Apr. 2010.

[29] J. W. Thornhill, J. L. Giuliani, J. P. Apruzese, A. Dasgupta, Y. K. Chong, B. Jones, A. J. Harvey-Thompson, D. J. Ampleford, S. B. Hansen, C. A. Coverdale, C. A. Jennings, G. A. Rochau, and M. E. Cuneo, "Two-dimensional RMHD modeling assessment of current flow, plasma conditions, and Doppler effects in recent Z argon experiments", IEEE Trans. Plasma Sci., vol. 43, no. 8, pp.2480–2491, 2015.

[30] J. L. Giuliani, J. W. Thornhill, E. Kroupp, D. Osin, Y. Maron, A. Dasgupta, J. P. Apruzese, A. L. Velikovich, Y. K. Chong, A. Starobinets, V. Fisher, Yu. Zarnitsky, V. Bernshtam, A. Fisher, T. A. Mehlhorn, and C. Deeney, "Effective versus ion thermal temperatures in the Weizmann Ne Z-pinch: Modeling and stagnation physics", Phys. Plasmas, vol. 21, no. 3, pp. 031209-1–031209-8, 2014.

[31] P. L. Coleman, D. C. Lamppa, R. E. Madden, K. Wilson,-Elliot, B. Jones, D. J. Ampleford, D. E. Bliss, C. Jennings, A. Bixler, and M. Krishnan, "Development and use of a two-dimensional interferometer to measure mass flow from a multi-shell Z-pinch gas puff," Rev. Sci. Instrum. vol. 83, no. 8, pp. 083116-01–083116-10, 2012.

[32] C. A. Jennings, D. J. Ampleford, D. C. Lamppa, S. B. Hansen, B. Jones, A. J. Harvey-Thompson, M. Jobe, T. Strizic, J. Reneker, G. A. Rochau, and M. E. Cuneo, "Computational modeling of Krypton gas puffs with tailored mass density profiles on Z", *Phys. Plasmas*, vol. 22, 056316-1–056316-10, May 2015.

[33] T. W. Hussey, N. F. Roderick, U. Shumlak, R. B. Spielman, and C. Deeney, "A heuristic model for the nonlinear Rayleigh–Taylor instability in fast Z-pinches," Phys. Plasmas, vol. 2, no. 6, pp. 2055–2062, Jun. 1995.

[34] K. G. Whitney, J. W. Thornhill, J. L. Giuliani, Jr., J. Davis, L. A. Miles, E. E. Nolting, V. L. Kenyon, W. A. Speicer, J. A. Draper, C. R. Parsons, P. Dang, R. B. Spielman, T. J. Nash, J. S. McGurn, L. E. Ruggles, C. Deeney, R. R. Prasad, and L. Warren, "Optimization of K-shell emission in aluminum Z-pinch implosions: Theory versus experiment," Phys. Rev. E, Stat. Phys. Plasmas Fluids Relat. Interdiscip. Top., vol. 50, no. 3, pp. 2166–2174, Sep. 1994.

[35] J. W. Thornhill, K. G. Whitney, J. Davis, and J. P. Apruzese, "Investigation of K-shell emission from moderate-Z, low-η (-velocity), Z-pinch implosions", J. Appl. Phys., vol. 80, no. 2, pp.710–718, Jul. 1996.

[36] D. Klir, P. Kubes, K. Rezac, J. Cikhardt, J. Kravarik, O. Sila, A. V. Shishlov, B. M. Kovalchuk, N. A. Ratakhin, V. A. Kokshenev, A. Yu. Labetsky, R. K. Cherdizov, F. I. Fursov, N. E. Kurmaev, G. N. Dudkin, B. A. Nechaev, V. N. Padalko, H.

Orcikova, and K. Turek, “Efficient neutron production from a novel configuration of deuterium gas-puff Zpinch”, Phys. Rev. Lett., vol. 112, no. 9, pp. 095001-1–095001-5, Mar. 2014.

Table I. List of double shell and triple (double shell + central jet) Ar gas puff shots discussed in the text.

Shot[a]	nozzle openings[b] r_N (cm)	mass distributions (mg/cm)	total linear mass m_ℓ (mg/cm)	pinch length ℓ (cm)	peak current I_{pk} (MA)	imp time Δt_{imp} (ns)	K-shell yield Y_K (kJ)	peak K-shell power P_K (TW)	K-shell FWHM Δt_K (ns)	Ref.
double-shell shots with the MPI 8 cm nozzle[3]										
Z663	1–2/3–4	.40/.40	0.800	2.4	15	112	274	14.4	12	[2]
Z1590	1–2/3–4	.435/.435	0.870	3.2	13.9	112	300	18.7	11	[4], [Apru_13]
double-shell shots with the AASC 8 cm nozzle[6]										
Z2381	1–2/3–4	.385/.615	1.0	2.5	13	107	250	16.5	9	[8]
Z2560	1–2/3–4	.385/.615	1.0	2.5	15	103	363	29	7.6	[9]
triple-shell shots with the TPSD 12 cm nozzle[12], [13]										
DE5417	2–3/5–6	.060/.060/0	0.120	3.8	3.57	210	9.7	0.87	5.5	[14]
DE5556	0.5/2–3/5–6	.054/.054/.027	0.135	3.8	3.46	205	21.2	1.65	7.3	[14]
DQ549	2–3/5–6	.174/.174/0	0.348	3.8	5.8	248	28	1.9	16	[16]
DQ563	0.5/2–3/5–6	.166/.166/.083	0.415	3.8	5.86	228	72	11.1	4.6	[13]

[a] Z for the Z pulsed power generator (Z663 and Z1560 were pre-refurbished Z shots); DE = Double Eagle; DQ = Decade Quad.

[b] Radii of nozzle openings, by convention from the axis outward, i.e., jet/inner shell/outer shell.

[c] Mass in each component outer shell/inner shell/jet. Note the opposite direction for the masses from the nozzle openings to follow the implosion description of "outer-on-inner-on-jet".

Table II. Gas-puff configuration and experimental results from Ref. [17] for four Ar shots on the Z generator. The pinch length was 2.5 cm. Simulation results from the Mach2-TCRE code are noted within parentheses.

Shot	gas-puff configuration (mg/cm)	total linear mass m_ℓ (mg/cm)	total yield Y_{tot} (kJ)	K-shell yield Y_K (kJ)	peak total power P_{tot} (TW)	peak K-shell power P_K (TW)	K-shell FWHM Δt_K (ns)
1:1.6 outer-to-inner shell mass ratio							
Z2560	0.385/0.616/0	1.0±10%	1005±20% (940)	363±9% (400)	40.0±20% (40)	28.5±10% (25)	7.4 (13)
Z2605	0.385/0.616/0.2	1.2±10%	1023±17% (1060)	373±9% (420)	63.3±20% (66)	32.0±10% (41)	7.6 (5.9)
1:1 outer-to-inner shell mass ratio							
Z2628	0.385/0.385/0	0.77±10%	436±17% (420)	153±9% (180)	9.0±20% (10)	6.1±10% (4.7)	36 (30)
Z2604	0.385/0.385/0.2	0.97±10%	894±17% (910)	375±9% (450)	44.8±20% (35)	33.1÷10% (25)	6.5 (21)

Table III. Properties of the simulations at the time of peak K-shell power.

Shot	He-like $16 \le \overline{Z} < 17$ (mg/cm)	H-like and stripped $Z > 17$ (mg/cm)	Ratio H-like/ He-like	m_K K-shell mass (mg/cm)	r_{CM} center-of-mass radius (cm)	r_{ind} inductive radius (cm)	r_K K-shell emitting radius (cm)	$\langle T_e \rangle_K$ average K-shell T_e (eV)	$E_{J\times B}$ coupled energy (kJ)	η*
	1:1.6 outer-to-inner mass ratio									
Z2560	0.112	0.421	3.76	0.533	0.30	0.3	0.29	2263	1030	4.3
Z2605	0.318	0.247	0.78	0.565	0.29	0.2	0.21	1782	1180	4.1
	1:1 outer-to-inner mass ratio									
Z2628	0.063	0.333	5.29	0.396	0.69	0.49	0.62	4597	823	4.4
Z2604	0.136	0.492	3.62	0.628	0.32	0.32	0.31	2271	1120	4.8
Z2628*	0.094	0.394	4.19	0.488	0.52	0.39	0.46	3374	960	4.0

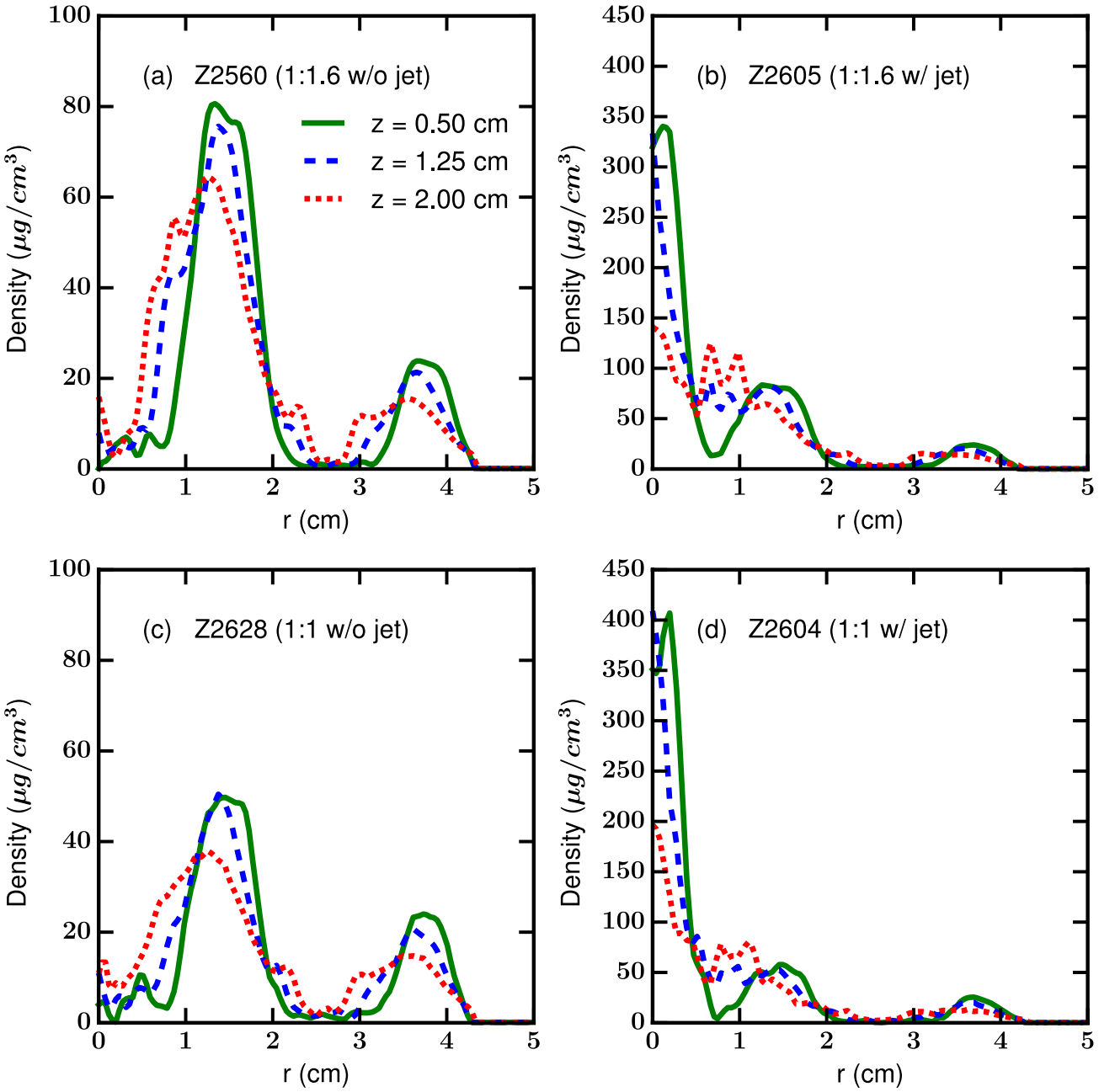

Fig. 1 Lineouts at three axial locations of the initial (r, z) mass density profile for the four Ar gas-puff configurations in Table I. The linear mass ratio of the outer:inner shell are listed along with the presence of absence of a central jet.

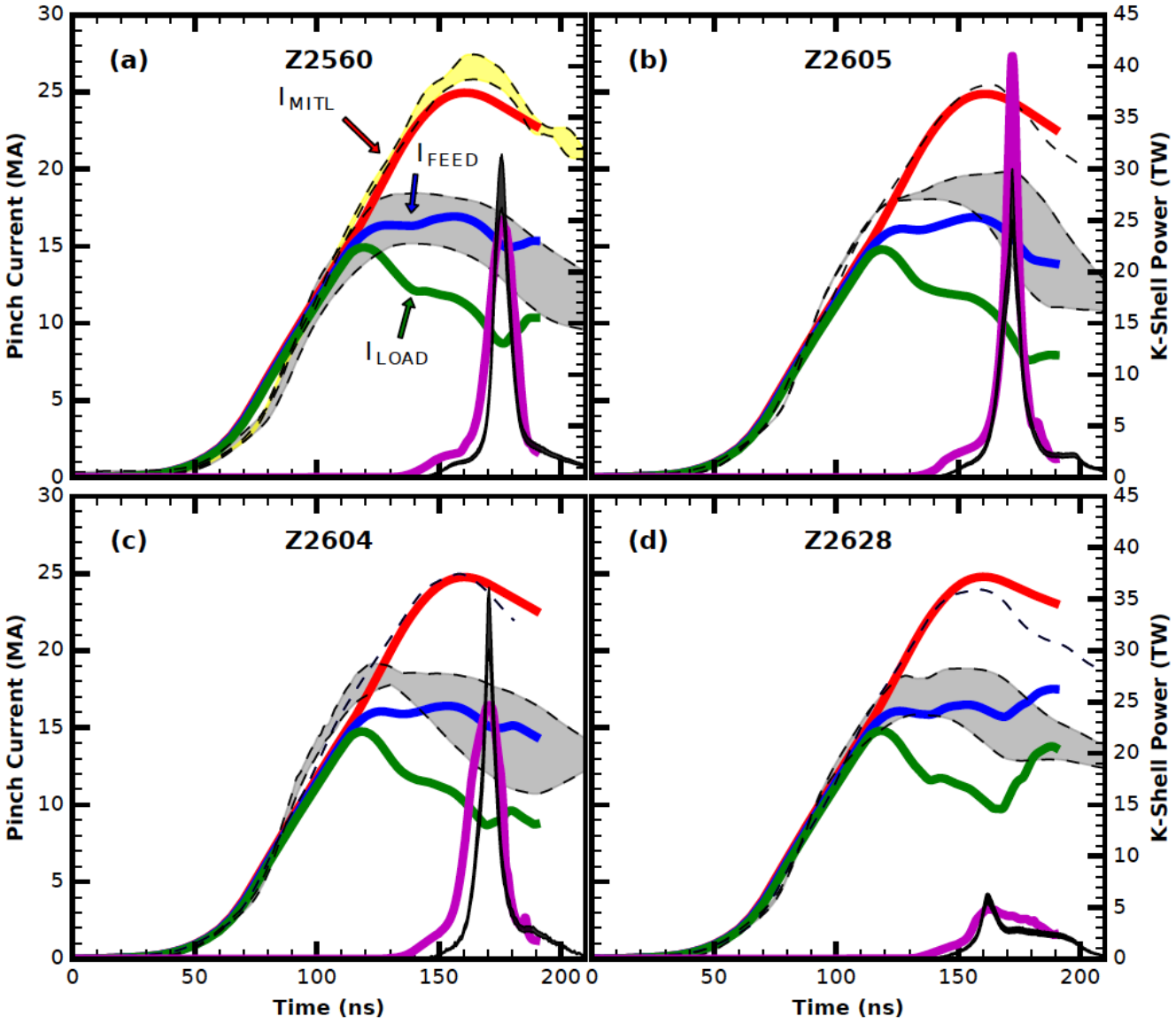

Fig. 2 Calculated MITL (solid red line), feed (solid blue line), and load currents (solid green lines) for the Ar shots in Table II. Shaded regions for the MITL and feed currents, and dashed line for the stack current are experimental values explained in the text. The calculated K-shell power pulse (solid purple line) is compared with the experimental data (narrow solid black) in each frame.

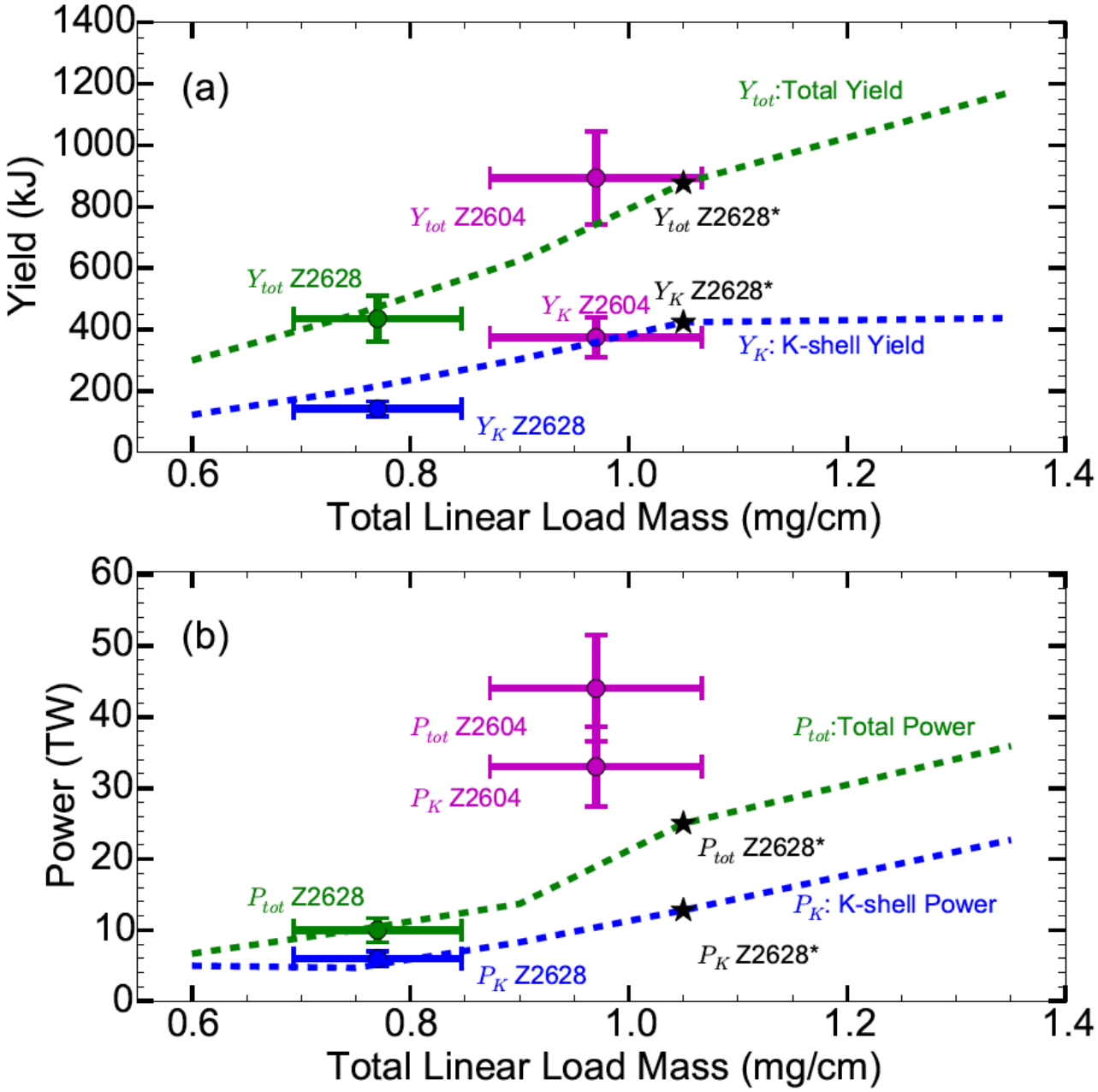

Fig. 3. (a) Total and K-shell yields from simulations for the density profile of Z2628 when the linear load mass is varied. (b) Same for the peak total and K-shell power. The experimental data for Z2628 and Z2604 from Table II are shown with error bars. For comparison with all the experimental data in Table II, the simulated Z2628* has Y_{tot} = 860 kJ, Y_K = 410 kJ, P_{tot} = 25 TW, P_K = 13 TW, and a K-shell pulse width of 25 ns.

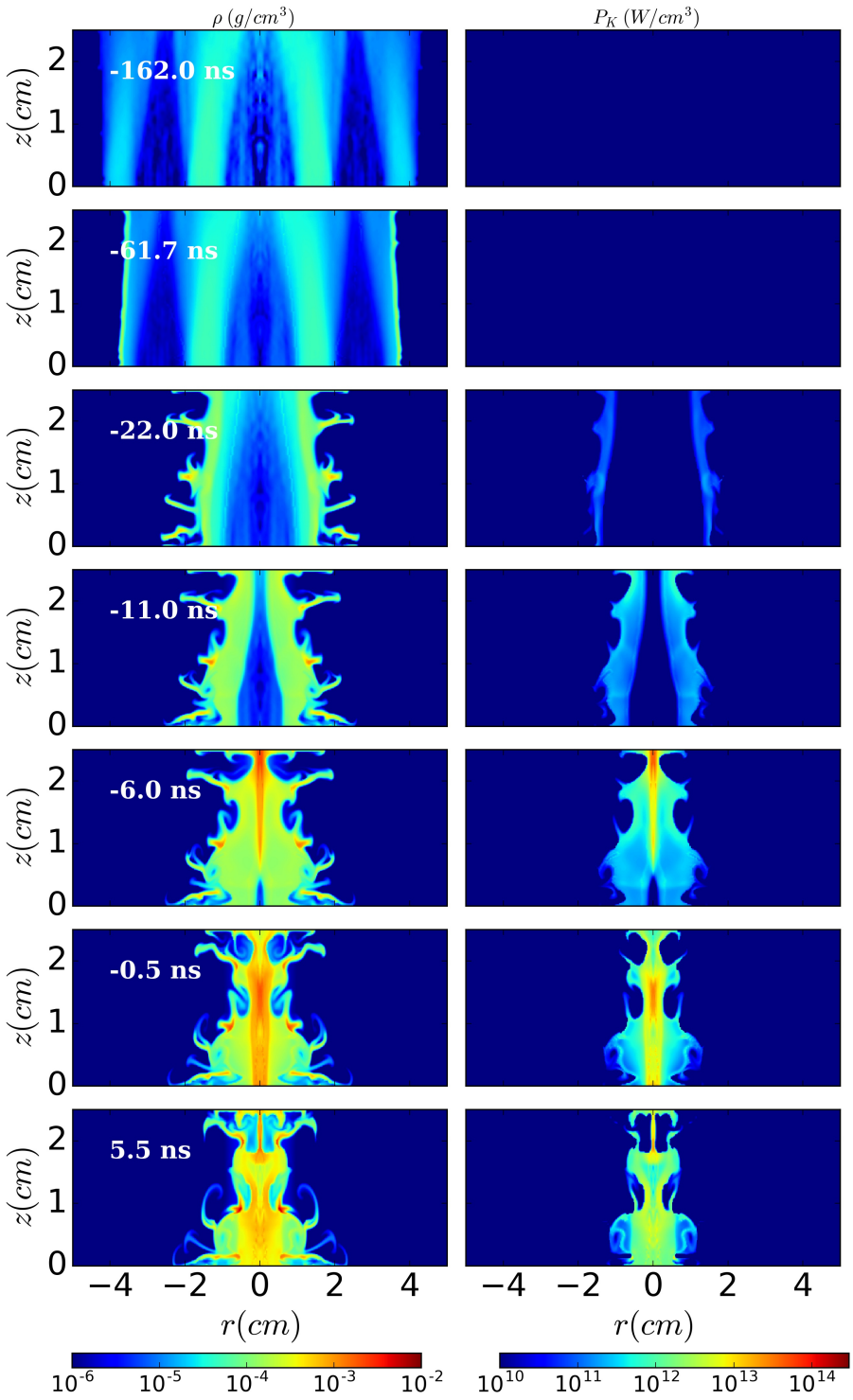

Fig. 4 Simulated evolution of the mass density (left) and K-shell radiation power density (right) for shot Z2628. The times are specified in this figure relative to the time of peak K-shell power.

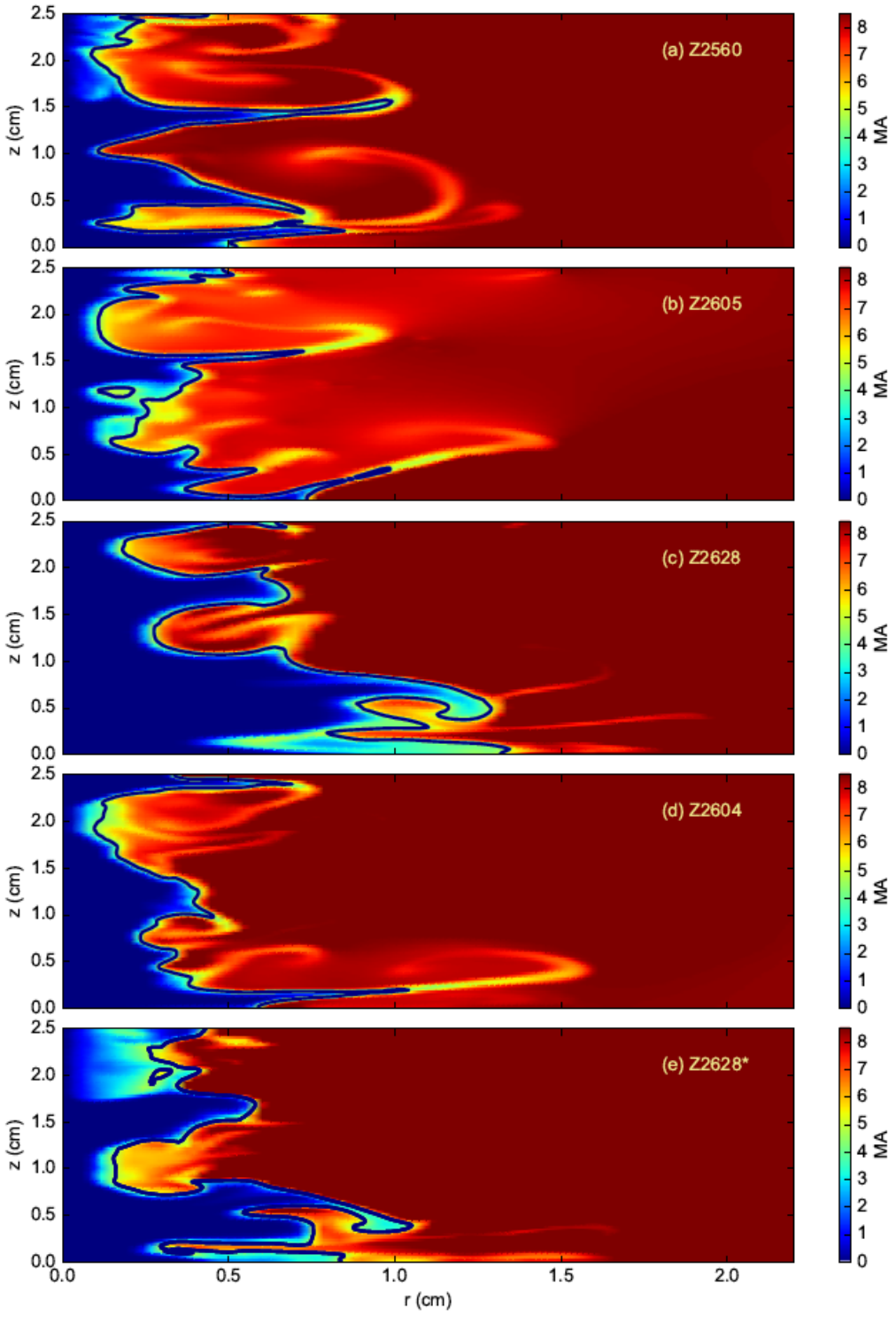

Fig. 5. Contour plot of the current (proportional to rB_{φ}) in the plasma calculated at the time of peak K-shell power for the shots in Table II and Z2628*. The solid blue line denotes the location of the 50% current level. From Fig.2 the load current at this time is 8 – 9 MA for all cases.

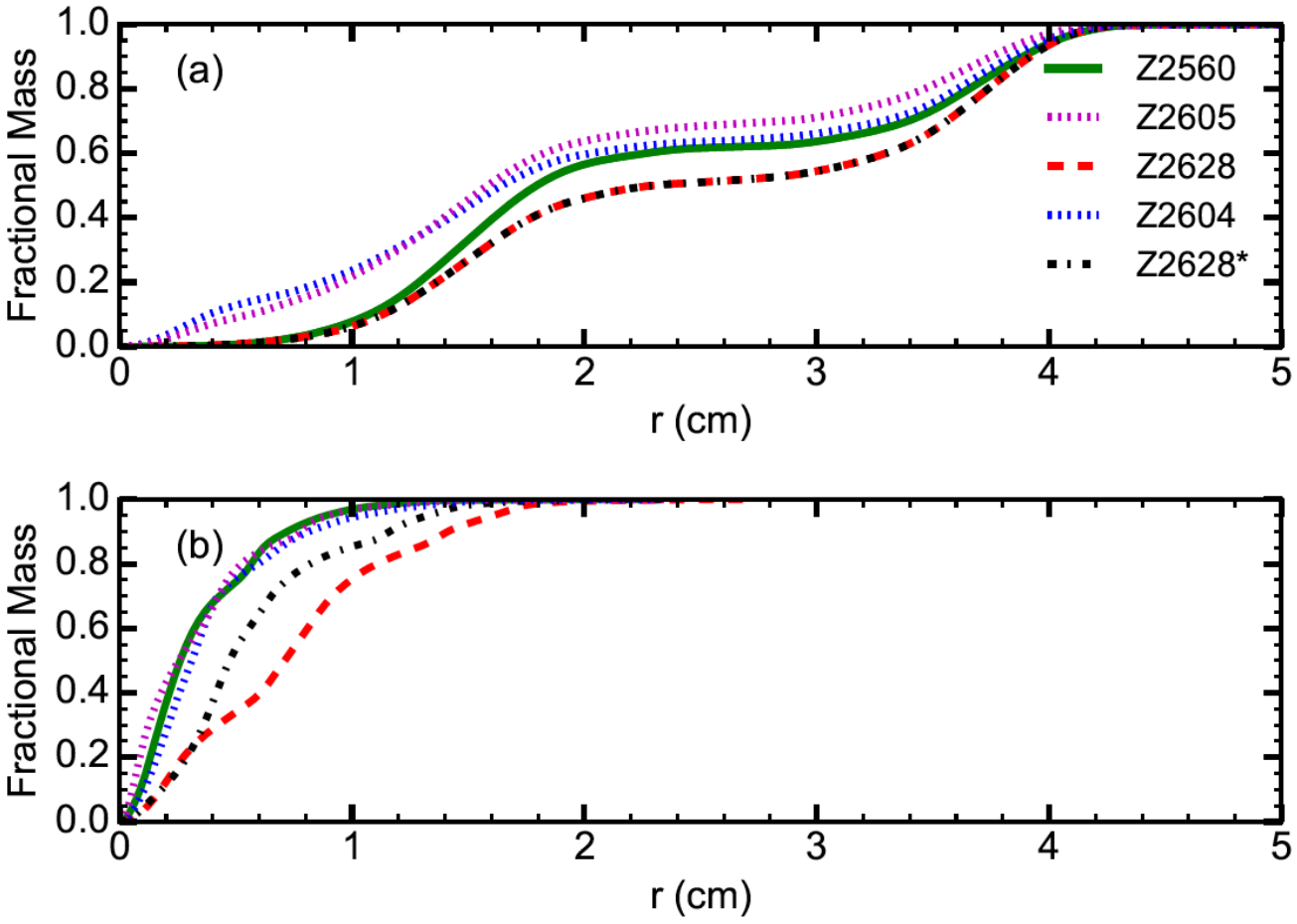

Fig. 6. (a) The normalized integral of the mass as a function of radius for the initial density profiles of the shots in Table II and Z2628*. (b) The same quantity at the time of peak K-shell power.

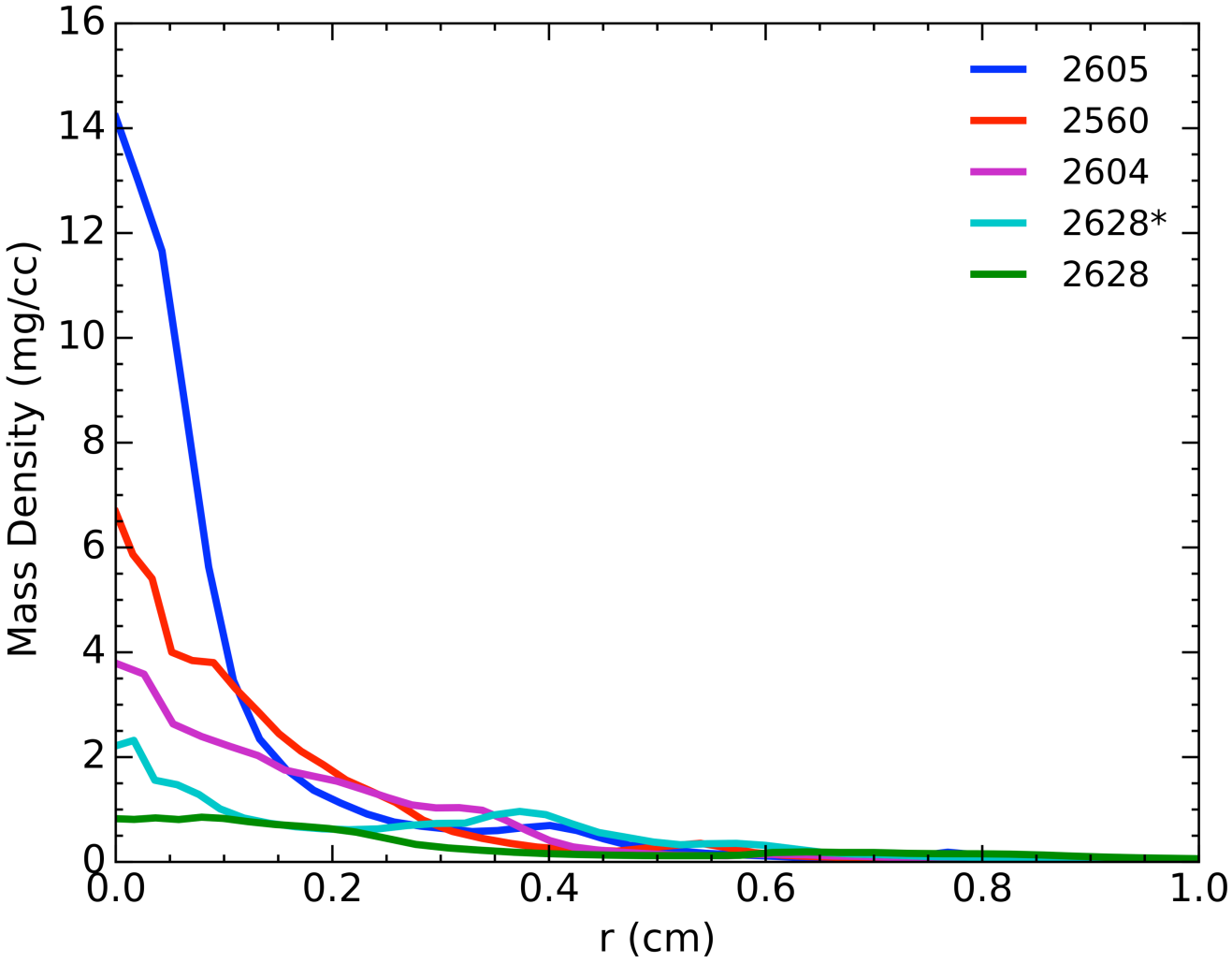

Fig. 7. The calculated radial mass density averaged along the axial direction at the time of peak K-shell power for the shots in Table II and Z2628*

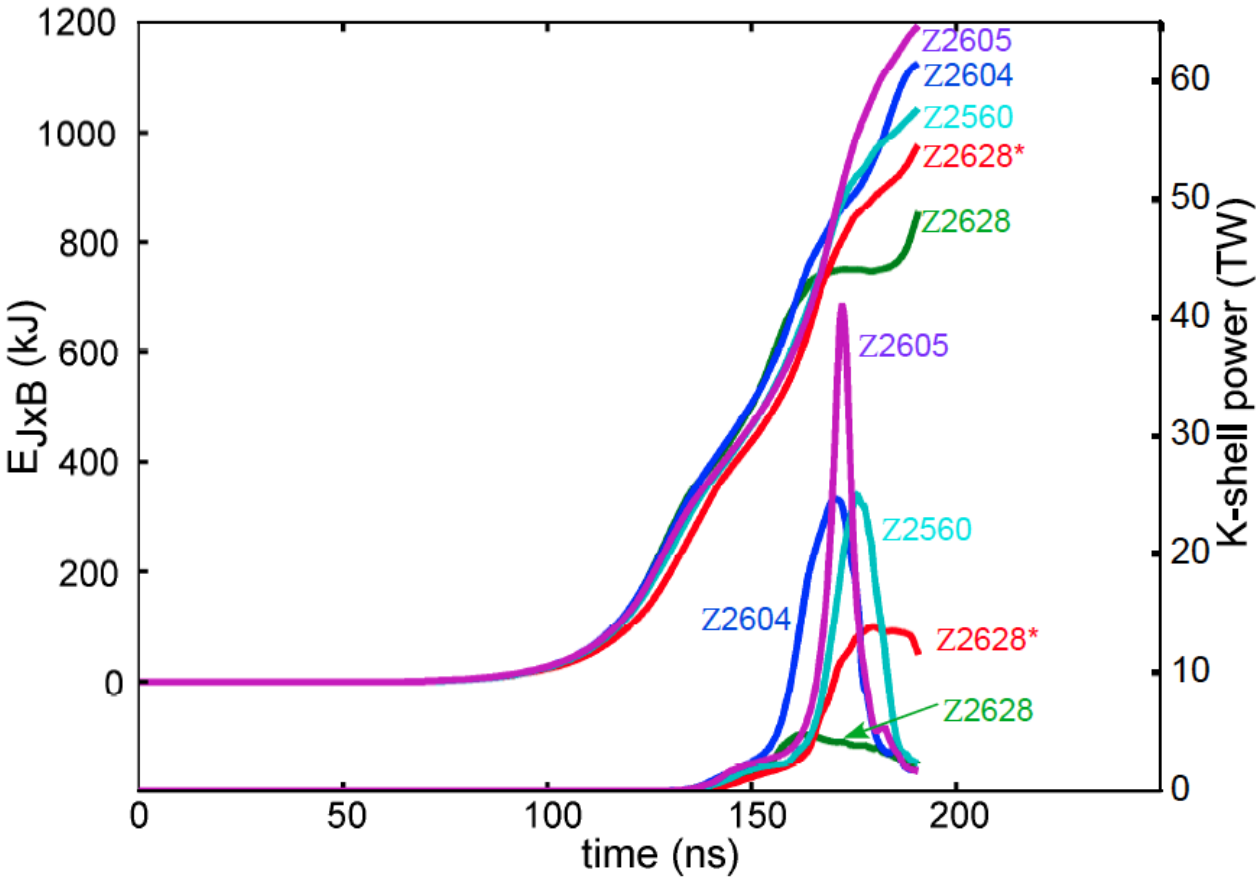

Fig. 8. The calculated coupled energy (E_{JxB}) from the Z generator during the implosion and throughout the stagnation for the shots in Table II and Z2628*. The calculated K-shell radiation pulses are added for comparison.